COMMUNICATION

Water-mediated surface diffusion mechanism enabling the Cold Sintering Process: A combined computational and experimental study

Mert Y. Sengul [a], Jing Guo [a][b], Clive A. Randall [a] and Adri C. T. van Duin *[c]

Abstract: Cold Sintering Process (CSP) densifies ceramics at extremely low temperatures relative to conventional sintering processes. Several ceramics and composite systems have been successfully densified under cold sintering; in the case of zinc oxide grain growth kinetics, reduced activation energies are shown, and yet, the mechanism behind this growth is unknown. Herein, we investigate these mechanisms in more detail with experiments and ReaxFF molecular dynamics simulations. We investigated the recrystallization of zinc cations at various acidic conditions and found that its adsorption to surface can be a rate-limiting factor for cold sintering. Our studies show that surface hydroxylation in CSP does not inhibit crystallization; in contrast, by creating a surface complex, it creates an orders of magnitude acceleration in surface diffusion, and in turn, accelerate recrystallization.

The need for sustainable processing is required to aid societal needs in reducing CO_2 emissions and lowering manufacturing costs; therefore, a protocol to produce high-quality ceramics through sintering at low temperatures and in faster times is of significant interest. The Cold Sintering Process (CSP) has been introduced as a non-equilibrium sintering approach that can densify ceramics at extraordinarily low temperatures ($T \leq 300°C$) and has been successful on over 70 inorganic materials [1]. The benefit of low-temperature sintering in CSP also has provided a process strategy to develop new materials, such as co-sintering of composite materials with ceramics and polymers, and nanocomposites with 2-dimensional materials in grain boundaries (GBs) [2]. Both the densification and grain growth kinetics of CSP are significantly accelerated relative to conventional sintering of equivalent materials, and zinc oxide (ZnO) is used as a model example, as there is extensive data using it in fundamental sintering studies. However, underlying mechanisms in CSP is unknown, and revealing these mechanisms will provide further understanding and aid in selection of the transient phases better enabling CSP.

To our knowledge, this investigation is the first to conduct an atomistic-level investigation to reveal details underpinning the CSP mechanisms. The evidence here demonstrates an accelerated surface diffusion as one of the mechanisms activated during CSP. Our findings could also be relevant to other water-assisted sintering techniques [3].

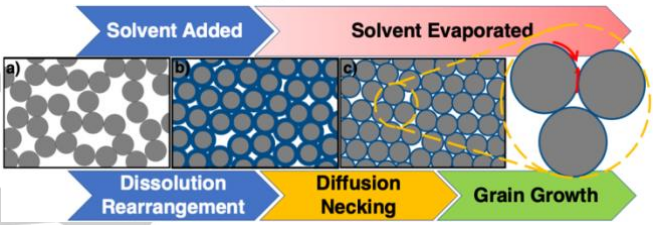

Figure 1. The visual representation of different stages of Cold Sintering Process.

The CSP assists densification of materials through dissolution/rearrangement and recrystallization processes in the presence of a transient phase. The qualitative interconnections of the relevant processes that underpin the sintering are outlined earlier [1]. The CSP first involves mixing of a small quantity of the solvent to the inorganic powder, which eliminates the solid/vapor interface as the liquid coats the grain surface (Figure1 a,b). The solvent type is crucial at this stage, as it controls kinetics and incongruent dissolution that can limit sintering and stoichiometric control through the microstructure. By applying external pressure and the dissolution of solute at the edges of a particle, the capillary pressure tends to rearrange the solid particles, which initiates densification. At the end of this first stage, a thin reactive liquid film separates densely packed solid particles. As a result of applied high pressure, high stresses are concentrated at the contact points in GBs. The stress concentration results in dissolution rates that are higher than the less stressed surfaces (e.g., pores), which creates a chemical potential gradient in the system. As a result, dissolved material diffuses through GBs either toward pore fluids or to less stressed surfaces of the grains at this second stage of CSP (Figure 1b). The adsorption of diffused material to surfaces is a rate-limiting factor at this stage [4] and may result in grain growth if successfully recrystallized. As the dissolved matter moves away from the contact points, the center-center distances between grains decrease, and further densification occurs [5]. With slightly elevated temperatures and uniaxial pressure, a simultaneously diffusive and reactive environment is yielded (Figure 1c). With the removal of the

[a] M. Y. Sengul, Dr. J., Guo, Prof. C. A. Randall, Prof. A. C. T. van Duin
Materials Research Institute
The Pennsylvania State University
University Park, PA, 16802, USA
E-mail: acv13@psu.edu
[b] Dr. J. Guo
State Key Laboratory for Mechanical Behaviour of Materials
School of Materials Science and Engineering
Xi'an Jiaotong University
Xi'an, China
[c] Prof. A.C.T. van Duin
Department of Mechanical Engineering,
The Pennsylvania State University,
University Park, PA, 16802, USA

Supporting information for this article is given via a link at the end of the document.

solvent from the system at the final stage, highly dense ceramics with extraordinary grain sizes are obtained under the CSP.

Several researchers reported water as an effective solvent in CSP, as it has a low boiling point, and is polar and relatively reactive to drive dissolution, and the diffusion through GBs in the second stage, to augment grain growth [1, 6]. However, the GB diffusion does not *per se* explain the previously observed extraordinary grain growth, since the growth substantially occurs during and toward the end of the solvent evaporation from the system (Figure 1c) [6a, 7]. Ideally, the water present in the system hydroxylates the surface. The hydroxylation of the surface reduces the surface energy and thereby lowers the sinterability. But interestingly, the reported CSP temperatures are not high enough for the surface dehydroxylation [7]. This apparent contradiction is examined here to explore the role of hydroxylation and its dynamics played under the CSP. To reveal the cause of extraordinary grain growths, we conducted a case study by combining experimental and computational methods for the ZnO/acetic acid/water system, which CSP is known to densify to 99%.

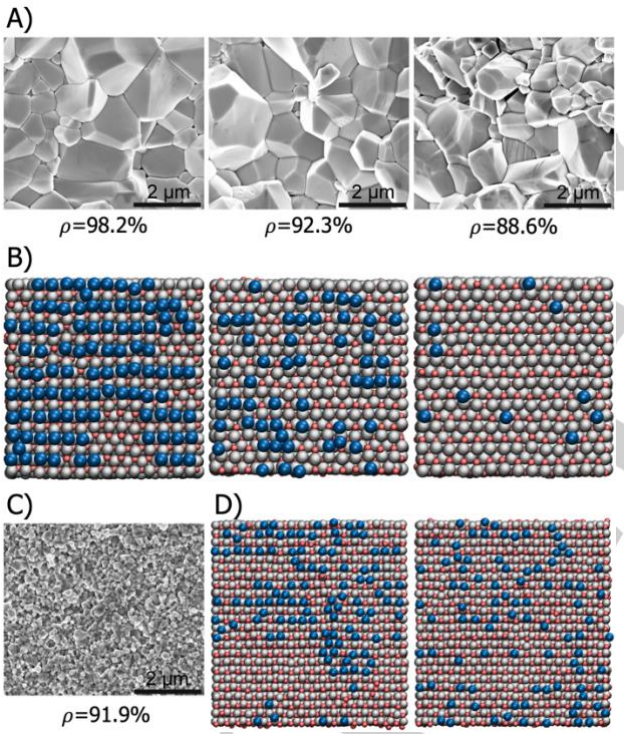

Figure 2. (A) SEM images of the microstructures of cold sintered samples using different acid concentrations and the bulk density values. Acid concentrations: Left - 2M, Middle – 4.6M, Right – 9M. The sintering temperature is 300°C. (B) The representation of crystallized Zn^{+2} ions from solution to lattice sites for different acid concentrations. Acid concentrations: Left - 2M, Middle – 4.6M, Right – 9M. (C) SEM image of the microstructure of a cold sintered sample and the bulk density value. The sintering temperature is 120°C, and the concentration is 2M. (D) Representation of crystallized Zn^{+2} ions from solution to lattice sites. The solvent is pure water (left) and 2M acetic acid-water mixture (right). Key: Zn^{+2} ion on the surface (blue); Oxygen atoms on the surface (pink); Oxygen atoms around migrating zinc (red); Hydrogen atoms (white); Surface zinc atoms (grey). The same colorization is used for all images. To increase visibility, larger versions images in B) and D) are given in supporting information.

Experiments were conducted by altering the acetic acid (HAc) concentration of the solvent while the solvent amount was kept constant. The HAc concentrations were selected as 2M, 4.6M, and 9M. Figure 2A shows the microstructures of ZnO pellets at various acid concentrations and the corresponding density values of each sample. Our experimental findings show that an increase in acidification of the solvent yields density and grain size reduction on the final pellet. The liquid amount in the system was kept constant to eliminate its impact on the diffusion rates. However, in contrast to expectations, the densification dramatically decreases despite constant liquid amounts and increased dissolution due to increased acidification, which implies a negative effect of excess HAc concentrations on the diffusion mechanisms activated in CSP. Once the HAc concentration yielding the highest grain size was determined (2M), the effect of operating temperature was investigated. When lower temperatures are considered (120°C instead of 300°C), low density and a drastic decrease in grain size were observed with the 2M HAc (Figure 2C). Residual acetate species were found in GBs, which low temperatures could not decompose (Figure S4) [7] and cause smaller grain development. In other words, it is hypothesized that the presence of residual acid species alters the interfacial chemistry, and in turn, prevents the activation of the diffusion mechanism enabling accelerated grain growth rates. Therefore, unveiling the inhibitory process could further aid explanations of the details underpinning the CSP mechanism. In the light of these experimental observations, in order to reveal the mechanism of CSP, we focused our modeling efforts on investigating the impact of acid concentration on interfacial kinetics at the atomistic level. We conducted molecular dynamics (MD) simulations using ReaxFF potential [8]. The ReaxFF is an MD procedure that is capable of modeling reactive liquid/solid interfaces at elevated temperatures and pressures. The ReaxFF force field parameters are optimized to reproduce energetics of reference reaction events which were obtained by using more accurate methods such as density functional theory. Note that ReaxFF may not reproduce reaction events that are not included during the parameter optimization process with same accuracy as reference reactions [9]; therefore, should be applied deliberately. The force field used in this study has been used in several different studies with similar chemistry and successfully reproduced relevant experimental results [10]. Systems in computational simulations were prepared to mimic experimental conditions by using the same acid concentrations. The initial atomistic system was prepared to represent the beginning of the final stage of CSP at which the system was assumed to be in thermodynamic equilibrium; thus, there is no chemical potential difference between the pore and the GB region (i.e., the dissolved material concentrations in the GB and the pore fluid are assumed to be equal and constant). Thereby, the simulation boxes involved ZnO surface and solvent molecules (water, HAc) saturated with a fixed number of dissolved Zn^{+2} ions. For details of computational studies, see supporting information. In order to decrease the liquid content, the systems were slowly heated up to the temperatures at which recrystallization starts.

The recrystallization simulation results can be seen in Figure 2B for different acid concentrations. The recrystallization trend is consistent with the densification and grain growth trends

observed in experiments. According to our simulations, as soon as the solvent meets the ZnO surface, a liquid/solid interface is formed with three layers (Figure S7): (1) hydroxide layer due to dissociation of water molecules on the surface, (2) structured water layer due to the interactions between water molecules and hydroxide layer, and (3) bulk solvent layer including dissolved Zn^{+2} ions. Due to the amphoteric behavior of ZnO surface, the hydroxide layer is composed of bridging and terminal hydroxyl groups. Recrystallization in the liquid/solid interface can be considered as a two-step dynamic process. First, an atom in solution approaches the surface and divests itself from the hydration shell to bind to the surface site. In the second step, the ion adsorbs to the surface site by replacing a surface specie. The activation barrier for this ligand exchange process is rate-limiting for grain growth. According to our simulations, in the 2M acid simulations, the crystallization of Zn^{+2} ions starts as soon as the outer water layer is removed from the surface, which corresponds to a temperature value of 150°C. We note that the temperature values in simulations tend to over-estimate exact temperatures due to the relatively short simulated timescales and needs to be considered not as absolute, but as relative trends.

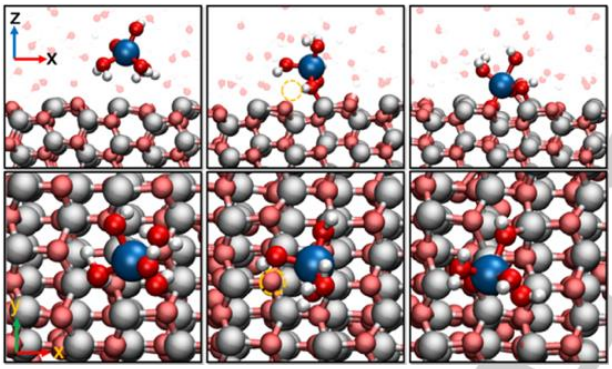

Figure 3. Visualization of ReaxFF simulations representing the Zn_{2+} ion crystallization on ZnO surface. Top and bottom panels show views from the side and above, respectively, at three simulation snapshots. Only the crystallized Zn^{+2} ion and the species 0.25 nm around this ion are shown for clarity. (left) Zn^{+2} approached to surface. (middle) Zn^{+2} is bonded to a bridging hydroxyl. (right) Zn^{+2} crystallized to vacant zinc site.

The approached Zn^{+2} ion first binds to the bridging hydroxyl (Figure 3). This process is observed to occur easily due to the hydrogen bonding interactions between the surface hydroxyls and the first hydration shell species around Zn^{+2} ion. We investigated the energy barriers of this binding process by applying a bond-restraint approach. (Supporting Information, Figure S1). When Zn^{+2} approaches the surface, the required energy for Zn^{+2} to divest itself from hydration shell and bind to the bridging hydroxyl was calculated as ~3 kcal. The adsorption energy is very small because Zn^{+2} can directly bind to the oxygen of the bridging hydroxyl due to the interaction between oxygen lone-pairs and divalent Zn^{+2} ion empty orbitals; therefore, there is no ligand exchange process for adsorption. Thus, hydroxylation of the surface does not reduce grain growth as typically expected. Instead, it very much aids the initial adsorption, which prevents recrystallization from limiting grain growth in CSP. However, it is observed to be different in the presence of an excess amount of HAc (4.6M and 9M) in the system. In the simulations, HAc molecules dissociate on the ZnO surface and bind to the positively charged surface sites, and when in excess, acetate molecules cover a significant part of the surface and tend to stay on the surface until elevated temperatures. Thus, this strong adsorption makes the exchange between the Zn^{+2} ions and acetate more difficult and delays recrystallization until elevated temperatures are reached. The number of HAc molecules that could be modeled in the simulation with 2M acid concentration was limited; therefore, in order to examine the difference between 0M and 2M HAc conditions, we extended our simulation sizes for these two specific cases (Figure 2D). As can be seen from the figure, no significant difference is observed in crystallization, because most of the HAc molecules bind to Zn^{+2} ions in the solution and do not cover the surface as happened in the 4.6M and 9M cases.

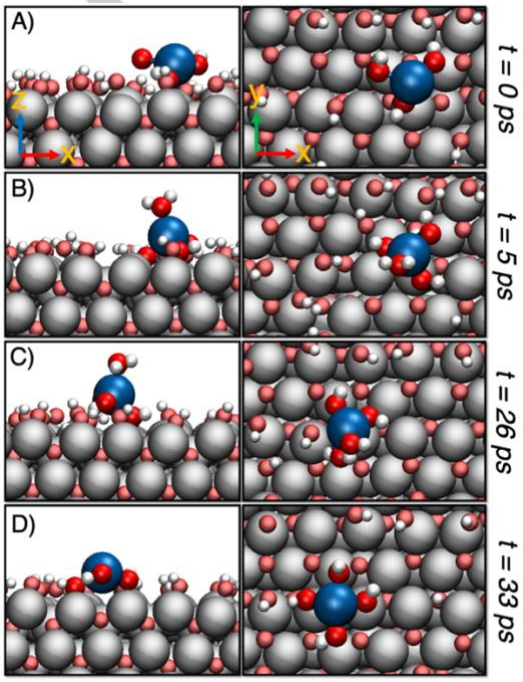

Figure 4. Visualization of ReaxFF simulations representing the Zn^{+2} ion diffusion on ZnO/water-vapor interface. Top and bottom panels show views from the side and above, respectively, at four simulation snapshots. Only the migrating Zn^{+2} ions and the species 0.25 nm around are shown for clarity in solution region. (A) Zn^{+2} ion adsorbed on surface. (B) Zn^{+2} ion attacked by water. (C) Zn^{+2} ion moved to the next site. (D) Zn^{+2} ion adsorbed on surface.

For the cases with lower acid concentrations, the adsorption of Zn^{+2} ion is not affected by the hydroxylation of the surface as discussed above, and it can be assumed that the surface behaves like a surface with a high vacancy concentration due to the presence of bridging hydroxyls and this structure results in an increase in surface diffusion. The vacancy-rich surface structures can be defined by the following quasi-chemical reaction:

$$Zn^{2+} + O^{2-} + H_2O \rightarrow Zn^{2+} + 2(OH^-) + V_{Zn} \quad (1)$$

In addition, and apart from the regular vacancy-enhanced surface diffusion, we observe an accelerated water-mediated surface

diffusion mechanism in our simulations. Figure 4 illustrates the simulation snapshots demonstrating the migration of a surface Zn^{+2} ion at the ZnO/water-vapor interface. Initially, the cation is bound to a bridging hydroxyl on the surface and coordinated by water molecules and/or hydroxides. As the simulation proceeds, an extra water molecule intermittently enters the first hydration shell of the Zn^{+2} ion. The presence of extra water molecule weakens the bonding between bridging hydroxyl and the Zn^{+2} ion and slightly levitates the ion, which results in the migration of Zn^{+2} ion to the next site (Movie S1). Since we observe the migration in the short (nanosecond scale) timescales amenable to ReaxFF-MD, it is safe to state that this mechanism yields an accelerated migration. The migration starts to be observed at 300°C in simulations; however, the surface is hydroxylated at these temperatures in the simulation environment; thus, the conditions can be assumed to correspond to lower experimental temperatures. Therefore, the surface diffusion mechanism can be activated in CSP during the evaporation of water or right before the evaporation ends, when trace amounts of water are still present. The proposed diffusion mechanism was observed in simulations both in the presence and absence of acetic acid. However, the surface complexation acts as a diffusion barrier and, depending on its magnitude, can affect the hopping of an ion from one site to the next. Therefore, the surface diffusion is perturbed by the presence of acetate (or residue) bound to the positively charged surface sites, forming a diffusion barrier. This finding accounts for smaller grain sizes, observed in experiments (Figure 2C) when residual acetate species are present in the GBs.

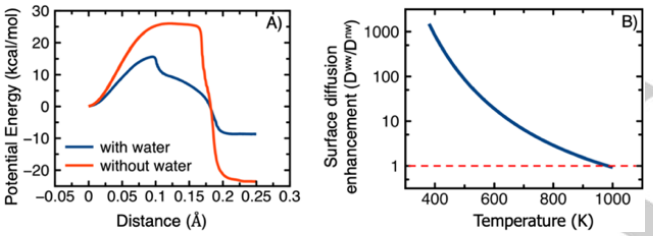

Figure 5. (A) The energy barriers for a jump of a Zn^{2+} ion to the next neighboring site on ZnO surface. The blue line is calculated in the presence of four water molecules around the cation, and the red line is calculated in the absence of water. For both calculations, ZnO surface is fully hydroxylated. (B) Surface diffusion enhancement with respect to temperature change, which is calculated using the Eq. (2).

The surface diffusion enhancement ($\mathcal{D}^*$) created by the presence of water can be approximated by Eq. (2), which was derived using the transition state theory. For details on its derivation, see supporting information.

$$\mathcal{D}^* = \mathcal{Z}\exp\left(\frac{-E_a^{ww}+E_a^{nw}}{RT}\right) \qquad (2)$$

where T, R, $\mathcal{Z}$ are temperature, gas constant and the partition function ratio, respectively. The energy barriers, E_a^{ww} and E_a^{nw}, correspond to the barrier for an atom to migrate to the next surface site in the presence and absence of water, respectively. The barrier energies were calculated using a sliding bond-restraint method [11] (see supporting information) (Figure 5A). The parameter $\mathcal{Z}$ is taken as 10^{-2} to include the lifting effect of water on the adsorbed cation (see supporting information). The surface diffusion enhancement created by water molecules disappears with increasing temperature and converges to unity at 983K (Figure 5B), which suggests that the observed water-mediated surface diffusion corresponds to diffusion values normally obtained at high temperatures.

In summary, we combined ReaxFF MD simulations and experiments to investigate the kinetics at the ZnO/HAc/water interface. We investigated the nature of the adsorption of the dissolved Zn-ions during CSP, and we found that the surface hydroxylation is not a bottleneck for the recrystallization to start. In fact, the hydroxylation aids the initial ion adsorption on the ZnO surface and also enhances the surface diffusion. In addition, we revealed an accelerated water-mediated surface diffusion that can be activated during CSP. The proposed mechanism can be activated for any material; however, it can be affected by several factors such as surface hydroxylation structure and the hydration energy of dissolved species, which are also effective on the adsorption as a rate-limiting factor. Therefore, these factors should be considered during the application of CSP. Apart from the acid concentration and temperature, pressure values in CSP could also have an impact on the system performance. High pressures applied in CSP form nanometer-scale GBs, which likely creates a complex regional confined space chemistry and influence diffusion; hence, such conditions should be further investigated.

Acknowledgements

A.C.T.v.D. acknowledges funding support from the Multi- Scale Fluid-Solid Interactions in Architected and Natural Materials (MUSE) Center funded by U.S. Department of Energy (DOE). C.R. acknowledges partial funding support from the Air Force Office of Scientific Research under Award No. FA9550-16-1-0429. M.Y.S. acknowledges partial funding support from U.S. National Science Foundation under Award No. DMR-1842922. The work presented herein was funded in part by the Advanced Research Projects Agency-Energy, U.S. DOE, under Award No. DE-AR0000766.

Keywords: Cold Sintering Process • Molecular Dynamics • ReaxFF • Surface Chemistry • Surface Diffusion

Entry for the Table of Contents

COMMUNICATION

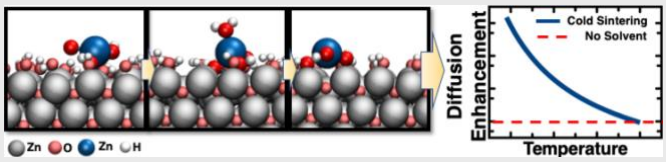

The presence of water can enhance the surface diffusion of ions at low temperatures and yields extraordinary grain growth in Cold Sintering Process, as revealed by ReaxFF molecular dynamics simulations.

*Mert Y. Sengul, Jing Guo, Clive A. Randall, Adri C.T. van Duin**

Page No. – Page No.

Water-mediated surface diffusion mechanism enabling the Cold Sintering Process: A combined computational and experimental study

[1] J. Guo, H. Guo, A. L. Baker, M. T. Lanagan, E. R. Kupp, G. L. Messing, C. A. Randall, *Angew Chem Int Ed Engl* **2016**, *55*, 11457-11461.
[2] a) J.-H. Seo, J. Guo, H. Guo, K. Verlinde, D. S. B. Heidary, R. Rajagopalan, C. A. Randall, *Ceram Int* **2017**, *43*, 15370-15374; b) J. Guo, N. Pfeiffenberger, A. Beese, A. Rhoades, L. Gao, A. Baker, K. Wang, A. Bolvari, C. A. Randall, *ACS Applied Nano Materials* **2018**, *1*, 3837-3844; c) J. Guo, B. Legum, B. Anasori, K. Wang, P. Lelyukh, Y. Gogotsi, C. A. Randall, *Adv Mater* **2018**, *30*, e1801846.
[3] a) A. Ndayishimiye, A. Largeteau, S. Mornet, M. Duttine, M.-A. Dourges, D. Denux, M. Verdier, M. Gouné, T. Hérisson de Beauvoir, C. Elissalde, G. Goglio, *Journal of the European Ceramic Society* **2018**, *38*, 1860-1870; b) J. Nie, Y. Zhang, J. M. Chan, R. Huang, J. Luo, *Scripta Materialia* **2018**, *142*, 79-82.
[4] T. Dewers, P. Ortoleva, *Geochim Cosmochim Ac* **1990**, *54*, 1609-1625.
[5] W. D. Kingery, *Journal of Applied Physics* **1959**, *30*, 301-306.
[6] a) J. Gonzalez-Julian, K. Neuhaus, M. Bernemann, J. Pereira da Silva, A. Laptev, M. Bram, O. Guillon, *Acta Materialia* **2018**, *144*, 116-128; b) F. Bouville, A. R. Studart, *Nat Commun* **2017**, *8*, 14655.
[7] S. Funahashi, J. Guo, H. Guo, K. Wang, A. L. Baker, K. Shiratsuyu, C. A. Randall, *Journal of the American Ceramic Society* **2017**, *100*, 546-553.
[8] S. D. Adri C. T. van Duin, Francois Lorant, and William A. Goddard III, *Journal of Physical Chemistry A* **2001**, *105*, 9396-9409.
[9] G. Saleh, C. Xu, S. Sanvito, *Angew Chem Int Ed Engl* **2019**, *58*, 6017-6021.
[10] a) Y. Yang, Y. K. Shin, S. Li, T. D. Bennett, A. C. T. van Duin, J. C. Mauro, *J Phys Chem B* **2018**, *122*, 9616-9624; b) M. Y. Sengul, C. A. Randall, A. C. T. van Duin, *ACS Appl Mater Interfaces* **2018,** 10, 37717-37724; c) D. Raymand, A. C. T. van Duin, D. Spångberg, W. A. Goddard, K. Hermansson, *Surface Science* **2010**, *604*, 741-752; d) D. Raymand, A. C. T. van Duin, M. Baudin, K. Hermansson, *Surface Science* **2008**, *602*, 1020-1031; e) D. Raymand, A. C. T. van Duin, W. A. Goddard, K. Hermansson, D. Spångberg, *J Phys Chem C* **2011**, *115*, 8573-8579.
[11] A. Vashisth, C. Ashraf, W. Zhang, C. E. Bakis, A. C. T. van Duin, *J Phys Chem A* **2018**, *122*, 6633-6642.